scientific reports

Check for updates

OPEN

Screening of rhizobacteria from monkey pod trees for plant growth promoters and evaluating the antifungal potential of the biosynthesized selenium nanoparticles

Abu M. Babajide[1], Gboyega E. Adebami[2]✉ & Bukola C. Adebayo-Tayo[1]✉

Rhizobacteria, residing in the root zone of plants, are essential for enhancing plant growth and development and have recently been recognized for their role in nanoparticle synthesis. This study aims to isolate new strains of rhizobacteria from monkey pod trees, evaluate their potential as plant growth promoters, and assess their ability to synthesize selenium nanoparticles (SeNPs) with antifungal properties. The objectives include screening the isolates for phosphate solubilization potential, indolic compound production, nitrogen fixation, and SeNPs synthesis. The best-performing isolates were identified through molecular techniques, and the synthesized SeNPs were characterized and tested for antifungal activity. Out of 30 rhizobacterial strains screened, isolates RS3E and RS3F, identified as *Lysinibacillus sphaericus* and *Bacillus amyloliquefaciens*, respectively, showed significant phosphate solubilization (PSI ranging from 2.0 to 3.80 mm) and Indole Acetic Acid (IAA) production. The greenly synthesized SeNPs exhibited a maximum absorption at 262 nm, with scanning and transmission electron microscopy confirming their spherical nature and average particle size of 16.704 nm. Further validation of SeNPs synthesis was achieved using Fourier transform infrared (FTIR) spectroscopy, X-ray diffraction (XRD), and energy dispersive X-ray (EDX) analysis. The SeNPs demonstrated excellent antifungal activity against *Aspergillus niger* and *Aspergillus flavus*, with inhibition zones ranging from 23.0 to 45.0 mm. This study highlights the potential of rhizobacteria-derived SeNPs as effective antifungal agents, offering a sustainable approach to fungal treatment in agriculture.

Keywords Antifungal agent, Indole acetic acid, Rhizobacteria, Phosphate solubilization index, Selenium nanoparticles (SeNPs)

Plant growth-promoting rhizobacteria (PGPR) are free-living bacteria that inhabit the rhizosphere and facilitate root development. Notably, *Bacillus* and *Pseudomonas* species are among the most prevalent PGPR[1]. These bacteria enhance plant growth through diverse mechanisms, including the production of phytohormones such as gibberellin, ethylene, indole-3-acetic acid (IAA), abscisic acid, and cytokinins, which play critical roles in plant development[2]. Additionally, PGPR improve iron availability through the production of siderophores and facilitate the solubilization of soil phosphorus via gluconic acid[3]. They also release volatile compounds that modulate plant signaling pathways, produce 1-aminocyclopropane-1-carboxylate (ACC) deaminase, which reduces ACC levels in salt-stressed plants, thereby alleviating the adverse effects of salinity on growth[2,4]. Furthermore, PGPR has been reported to function as biocontrol agents by reducing the populations of root pathogens and other detrimental microorganisms in the rhizosphere, thereby supporting plant health and growth[1,5]. They can also fix atmospheric nitrogen in association with plant roots[5–8].

[1]Department of Microbiology, University of Ibadan, Ibadan, Oyo State, Nigeria. [2]Department of Biological Sciences, Mountain Top University, Ibafo, Ogun State, Nigeria. ✉email: gboyega.adebami@gmail.com; bukola.tayo@gmail.com

PGPR are known for their symbiotic relationship with Monkey pod trees also known as *Samanea saman* which is a tropical leguminous tree native to Central and South America[9]. The monkey pod tree, known for its symbiotic relationship with plant growth-promoting rhizobacteria (PGPR), offers numerous benefits beyond this ecological interaction[10]. Its wood is highly prized for its durability and distinctive chocolate-brown hue, making it a valuable resource for fine furniture, cabinetry, millwork, decorative veneers, joinery, and turning projects. Additionally, the monkey pod tree serves as an ornamental plant, with its expansive canopy providing shade and cooling the surrounding ground. This feature makes it an ideal choice for planting in pastures, along roadsides, and in parking lots, offering a natural respite from the sun's heat[11].

Selenium nanoparticles (SeNPs) synthesized from plant growth-promoting rhizobacteria (PGPR) hold great promise for sustainable agriculture and plant health, as they have been shown to enhance plant growth, improve nutritional quality, and mitigate environmental stress[12]. The production of SeNPs from PGPR involves a biofabrication process that harnesses the unique properties of these beneficial bacteria[13]. PGPR play a crucial role in reducing selenium ions to elemental selenium, leading to the formation of SeNPs with enhanced bioavailability and low toxicity[14]. The biofunctionalized SeNPs derived from PGPR exhibit superior antioxidant activity compared to conventional selenium forms, making them ideal for promoting plant growth and combating oxidative stress[13,15].

Fungal pathogens are among the most significant threats to plant health, causing diseases that result in substantial agricultural losses worldwide. They invade plant tissues through spores or mycelia, often thriving under warm and humid conditions[16]. Common fungal diseases include Fusarium wilt, caused by *Fusarium oxysporum*, which disrupts vascular systems, and powdery mildew, caused by *Erysiphe* species, affecting photosynthesis[17]. Other notable pathogens include *Aspergillus* and *Alternaria* species, known for their toxin production and crop contamination. *A. niger* and *A. flavus* are known for causing post-harvest diseases in fruits, vegetables, and nuts, with *A. niger* leading to black mold on crops like onions and grapes, and *A. flavus* producing aflatoxins, potent carcinogens, particularly in peanuts and corn[18].These fungi damage plant growth, yield, and quality, necessitating integrated management strategies such as resistant cultivars, fungicides, biological control agents, and environmentally friendly nanoparticle-based approaches[19].

The antifungal properties of the synthesized SeNPs from PGPR have garnered significant research interest as these exceptional capabilities make them a promising alternative for managing various fungal species[20]. For instance, SeNPs obtained by plant-mediated synthesis have demonstrated antifungal activity against various plant pathogens, including *Fusarium oxysporum*, *Colletotrichum gloeosporioides*, *Oligoporus pelliculosus*, *Alternaria alternata*, *Phytophthora capsid* and *Botrytis cinerea*[21–23]. The antifungal activity of SeNPs has been greatly influenced by its nanoparticle size and bioavailability, with smaller SeNPs demonstrating better activity[22,23].

Therefore, this study aims to explore the dual potential of rhizobacteria isolated from the Monkey Pod Tree rhizosphere as plant growth promoters and synthesizers of SeNPs with antifungal properties. The objectives include isolation and screening of rhizobacteria from the rhizosphere of the Monkey Pod Tree for their potential to promote plant growth. Investigate the produced metabolites for the biosynthesis of SeNPs, characterize the synthesized SeNPs using various analytical techniques, and evaluate the antifungal activity of the biosynthesized SeNPs against specific phytopathogens, including *F. oxysporum*, *Aspergillus niger*, and *Aspergillus flavus*.

Methodology

Samples collection and isolation of rhizobacteria

Soil samples were randomly collected from the rhizosphere of the monkey pod tree in the Ibadan metropolis, following the methodology established by Kaur et al.[24] for isolating plant growth-promoting rhizobacteria. These samples were subsequently transported to the lab for further analysis. The isolation of the PGPR from the soil samples was conducted using the standard dilution pour plating technique on King B medium, as outlined by Ambrosini and Passaglia[25], after performing serial dilutions of the samples. The cultures were incubated at 35 °C for duration of 24 h.

Screening for plant growth promoting properties

Determination of phosphate solubilization potential

The isolates were evaluated for their phosphate solubilization capabilities using Pikovskaya (PVK) medium, following the protocol established by Nautiyal[26]. This medium contained (g/L): 10.0 glucose; 0.5 $(NH_4)_2SO_4$; 0.1 $MgSO_4.7H_2O$, 0.002 $MnSO_4.H_2O$, 5.0 $Ca_3(PO_4)_2$, 0.2 NaCl, 0.2 KCl, 0.002 $FeSO_4.7H_2O$, 0.5 yeast extract, and 15.0 agar-agar in 1.0 L of distilled water. The pH was adjusted to 7.0 before sterilization at 121 °C for 15 min. Each bacterial isolate was spot-inoculated at the center of the agar plates and incubated at 25 °C for 7 days. Phosphate solubilization was indicated by the formation of transparent halos around the bacterial colonies. On the seventh day, the phosphate solubilization index (PSI) was calculated by measuring the diameters of the clear zones and colonies in millimeters, as outlined by Elias et al.[27]. The PSI was calculated as follows:

$$\text{PSI} = \frac{\text{colony diameter} + \text{halo zone diameter}}{\text{Colony diameter}}$$

Quantitative determination of phosphate solubilization ability of isolates

Bacterial isolates with a PSI above 2.0 were selected for further analysis in liquid medium using PVK broth, with calcium phosphate as the phosphate source. The broth was prepared, pH-adjusted to 7.0, and sterilized at 121 °C for 15 min. Each bacterial suspension (1 mL, standardized to 0.5 McFarland) was inoculated into 50 mL conical flasks containing 20 mL of PVK broth and incubated at 180 rpm for 7 days at 27 °C. After incubation, the supernatant was separated by centrifugation at 6000 rpm for 10 min. Soluble phosphate concentration was measured colorimetrically via the reduction of a phosphorus-molybdate complex, producing a blue color

proportional to the phosphorus concentration [28]. For measurement, 1 mL of filtrate was mixed with 4 mL of distilled water and 5 mL of solution AB (solution A contains 2.5 g sodium molybdate in 100 mL of 10 N H_2SO_4, while solution B contains 0.15 g hydrazine sulfate in 100 mL of distilled water), incubated at 50 °C for 10 min, then cooled. Optical density was determined at 825 nm using a spectrophotometer (Unico, S-2150). Experiments were conducted in triplicate, and phosphate concentration was calculated using a standard curve from KH_2PO_4 solutions (0 to 2 mg/L).

Determination of Indolic compounds production by the isolates

The production of indolic compounds was evaluated by culturing the isolates in King-B broth medium. Following incubation, bacterial cells were separated by centrifugation at 6000 rpm for 3 min. Subsequently, 1 mL of the supernatant was combined with 2 mL of Salkowski's reagent (10 mM $FeCl_3$ in 35% perchloric acid) and two drops of orthophosphoric acid, across three biological replicates. The mixture was then incubated in the dark at room temperature for 30 min. The presence of indole-3-acetic acid (IAA) was indicated by a red coloration[29]. IAA quantification was achieved by measuring absorbance at 530 nm, using uninoculated LB medium as a baseline. The IAA concentration was determined from a standard curve of indole-3-acetamide (10–60 µg/mL), also in triplicate.

Determination of nitrogen fixing activity of the isolates

The isolates were cultured on King-B solid medium and then transferred to LGI-P (Low Glycemic Index-P) nitrogen-free semi-solid medium. The vials were incubated at 28 °C for 4 to 7 days, during which a veil-like pellicle formed on the medium's surface, signifying the presence of nitrogen-fixing bacterial isolates.

Molecular identification of the selected isolates

Bacterial isolates were identified via 16 S rDNA sequencing. The target region of the 16 S gene was amplified using 2X Master Mix (OneTaq® Quick-Load®; NEB Catalogue No. M0486). Primers 16–27 F and 16 S-1492R were utilized for this amplification. The PCR protocol consisted of 30 cycles: initial denaturation at 95 °C for 5 min, denaturation at 94 °C for 1 min, annealing at 60 °C for 1 min, extension at 72 °C for 1.5 min, followed by a final extension at 72 °C for 10 min, and a hold at 4 °C. PCR products (50 ng/µL) were analysed by Inqaba Biotec, South Africa, for molecular identification. The 16 S rDNA sequences were analyzed using the GenBank database and BLAST for nucleotide homology. A phylogenetic tree was constructed with the neighbor-joining method in MEGA 11 (version 11.0.13), using 1000 bootstrap replications for statistical support[30].

Determination of antifungal activity of the bacterial isolates

The isolates were cultivated in King-B liquid medium until they reached the stationary phase. The cell-free supernatant was then extracted by centrifugation at 6000 rpm for 10 min. Following the methodology of Fardsadegh and Jafarizadeh-Malmiri [31], the antifungal properties of the supernatant were assessed. A 1 mL suspension of fungal spores (*Fusarium oxysporum*, *Aspergillus niger*, and *Aspergillus flavus*) at a 0.5 McFarland standard was inoculated onto PDA agar plates. Using a sterile cork borer, five wells of 5.0 mm diameter were created, and 50 µL of the supernatant was introduced into each well. The diameters of the inhibition zones were determined after the incubation at 25 °C for 48 h.

Biosynthesis of selenium nanoparticles (SeNPs)

The production of selenium nanoparticles was conducted as described by Fardsadegh and Jafarizadeh-Malmiri [31]. Bacterial cultures were grown in King B liquid medium for 72 h. after which the cells were separated from the growth medium by centrifugation at 6000 rpm for 10 min to obtain the cell-free supernatant. A 10 mM sodium selenite (Na_2SeO_3) solution was prepared by dissolving 0.263 g of its salt in 100 mL of distilled water. Different volumes of the bacterial cell-free supernatant (ranging from 5 to 15 mL) were combined with varying amounts (10 to 30 mL) of the sodium selenite solution. The resulting reaction mixtures were then incubated at 35 °C for a period of 3 days.

Characterization of the Greenly synthesized (SeNPs)

Visual observation

The gradual colour change of the reacting mixture in Erlenmeyer flask was visually observed and recorded.

UV-visible spectroscopy

UV-Visible spectroscopy was conducted using PerkinElmer Lambda 950 UV/Vis spectrometer[32], which involved monitoring the reduction of selenium ions in the reaction mixture by measuring optical density. A 2.0 mL aliquot of the colloidal solution was placed in a cuvette, and the wavelength was scanned between 200 and 700 nm, with control samples serving as references.

Scanning electron microscopy (SEM)

SEM was utilized to examine the surface morphology of SeNPs. After a 6-hour reaction period, the colloidal solution was centrifuged at 14,500 rpm for 4 min. The precipitate was resuspended in sterile water, centrifuged, and washed by repeating this process three times, followed by a final acetone rinse. The purified selenium nanoparticles were then sonicated for 10 min to form a suspension. A drop of this suspension was placed on a carbon-coated copper grid and dried under a lamp. The sample was analyzed using a Jeol JSM-690 A Analytical SEM[32].

Transmission electron microscopy (TEM)
Bacterial cells were cultivated using the optimal selenite concentration. Before centrifugation, samples of these cells were placed onto nickel or copper grids coated with a 1% formvar solution in 1.2-dichloroethane. TEM images were then captured using a NanoMill transmission electron microscope[33].

Fourier-transform infrared (FTIR) spectroscopy
The functional groups responsible for the reduction and stabilization of SeNPs were identified using Shimadzu IR double beam spectrophotometer (UV-1900i) to acquire the FTIR spectrum. The potassium bromide (KBr) pellet method, with a 1:30 ratio of nanoparticles to KBr, was employed for analysis. The spectrum was recorded in transmittance mode at a resolution of 4 cm^{-1}, with peaks plotted on the X-axis and wave numbers (cm^{-1}) on the Y-axis. The spectrum, recorded over a range of 350–4000 cm^{-1}, was analyzed by subtracting the pure KBr spectrum[34].

X-ray diffraction (XRD) spectroscopy
The quality and crystallinity of the synthesized compounds were evaluated using an X-ray diffractometer (X'Pert PROPAN Analytical, Europe). The SeNPs were first centrifuged at 1400 rpm and 8 °C for 15 min followed by filtration. The resulting precipitate was washed three times with ethanol and then rinsed with sterile distilled water in three additional cycles. The purified nanoparticles were dried at 60 °C and subsequently ground into a fine powder using a ceramic mortar and pestle. This powdered sample was analyzed at temperature range of 20 °C to 80 °C [35].

Energy dispersive X-ray (EDX) spectroscopy
Elemental selenium and other capping agents were identified in the sample through EDX analysis using a Philips CM200 200 kV TEM. The atomic percentage of metals determined through EDX analysis confirms the sample's purity and elemental composition[36]. This same sample was also utilized for TEM analysis.

Antifungal activity of sodium selenite and senps
The antifungal potentials of sodium selenite dissolved in distilled water and the greenly synthesized SNPs was evaluated. The three fungal cultures (*F. oxysporum*, *A. niger*, and *A. flavus*) used in this study was collected from the mycology research group of Mountain Top University. 1 mL 0.5 McFarland standard of each fungal spore suspension was prepared and inoculated onto PDA agar plates. A sterile cork borer was used to create 5 mm diameter holes on the inoculated PDA plates. 50 µL of sodium selenite solution, RS3E-SeNP, and RS3F-SeNP suspensions were then pipetted into separate holes on the plates. The plates were incubated at 25 °C for 48 h after which the clear zones around the holes were measured and recorded [37].

Statistical analysis
The experimental data obtained from this study were analyzed using IBM SPSS (version 25.0) to ensure the validity and reliability of the results. Analysis of variance (ANOVA) was employed to evaluate the significance of variations among the tested groups. Where ANOVA indicated significant effects ($p \leq 0.05$), a post-hoc analysis using Tukey's Honest Significant Difference (HSD) test was conducted to determine specific group differences. All experiments were performed in triplicates.

Results
Isolation of rhizobacteria from the soil sample
A total of thirty (30) rhizobacterial strains were isolated from six different rhizosphere samples obtained from Monkey Pod tree within Ibadan metropolis. Some of the screened isolates demonstrated the ability to solubilize phosphate on Pikovskaya's (PVK) medium, evidenced by the formation of distinct halo zones as shown in Fig. 1.

Screening the isolates for phosphate solubilization potential
Eight (8) isolates showed phosphate solubilization potentials. There was significant difference ($P \leq 0.05$) in the Phosphate Solubilization index (PSI) as the values ranged from 2.00 ± 0.01^{e} to 3.83 ± 0.03^{a} (Table 1). Isolate RS3F exhibited the highest halo diameter (23.0 mm) and PSI (3.83), followed by isolate RS3E (19.0 mm and 2.92), while isolate RS4B had the lowest values (12.0 mm and 2.00)."

Quantitative analysis of phosphate solubilization
Based on the qualitative analysis of tricalcium phosphate solubilization, all the isolates that were able to solubilize the phosphate source were analysed for their phosphate-solubilizing ability in PVK liquid medium. The bacterial isolates released soluble phosphorus from $Ca_3(PO_4)_2$ at concentrations ranging from 2.08 ± 0.02^{e} to 3.10 ± 0.05^{a} µg/L as shown in Table 2. Isolate RS3F had the highest phosphorus concentration (3.10 µg/L) followed in order by isolate RS3E (3.07 µg/L) while isolate RS4D had the lowest (2.08 µg/L).

Qualitative and quantitative analysis of Indole acetic acid (IAA) production
The assessment of bacterial isolates for IAA production in King-B liquid medium revealed the development of a pink colour, which is indicative of indolic compound synthesis as shown in Fig. 2. There was significant difference in the IAA production as eight of the 30 isolates were able to produce IAA ranging from 0.339 ± 0.01^{d} to 1.182 ± 0.03^{a} µg/mL as shown in Table 3. Isolate RS3F had the highest while RS4C had the least concentration.

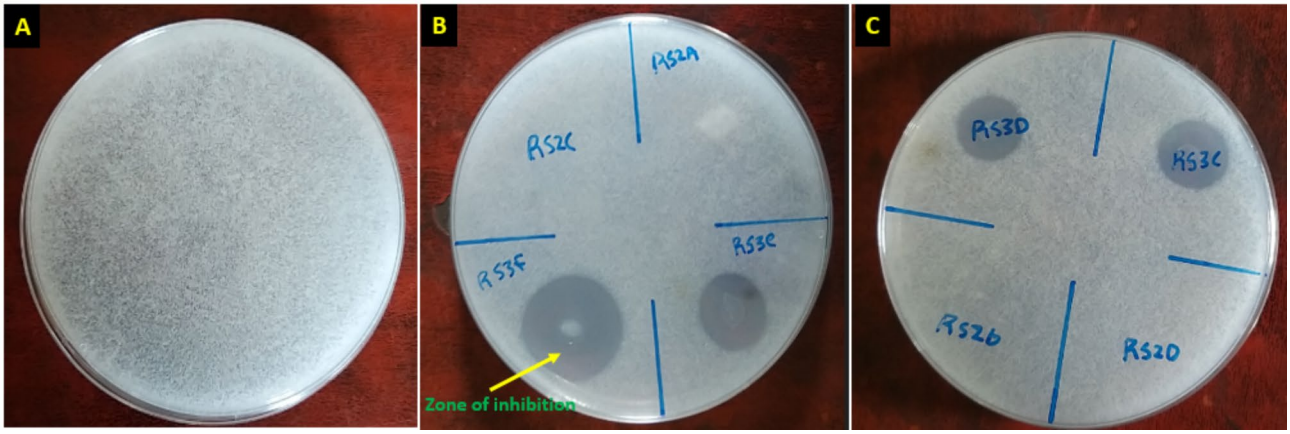

Fig. 1. Representative plates showing halo zones of phosphate-solubilization on PVK medium. Code: (**A**) Control plate showing a white translucent layer indicative of insoluble tricalcium phosphate. (**B**) PVK plate showing halo zones around isolate RS3F and RS3E.

Isolate code	Colony Diameter (DC) (mm)	Diameter of halo (DH) (mm)	PSI (DH/DC ratio)
RS3B	7.0 ± 0.03^{a}	16.0 ± 0.11^{c}	2.29 ± 0.01^{d}
RS3C	6.0 ± 0.01^{b}	15.0 ± 0.08^{cd}	2.50 ± 0.02^{c}
RS3D	5.0 ± 0.02^{c}	14.0 ± 0.10^{d}	2.80 ± 0.02^{b}
RS3E	6.5 ± 0.04^{b}	19.0 ± 0.12^{b}	2.92 ± 0.01^{b}
RS3F	6.0 ± 0.02^{b}	23.0 ± 0.11^{a}	3.83 ± 0.03^{a}
RS4B	6.0 ± 0.02^{b}	12.0 ± 0.11^{e}	2.00 ± 0.01^{e}
RS4D	7.0 ± 0.02^{a}	18.0 ± 0.09^{b}	2.57 ± 0.02^{c}
RS5D	6.0 ± 0.01^{b}	15.0 ± 0.08^{cd}	2.50 ± 0.01^{c}

Table 1. Qualitative analysis of Phosphate-Solubilization bacteria on GY/Tricalcium phosphate medium. Mean values in each vertical column with the same lowercase letter(s) are not significantly different using Duncan's Multiple Range Test at $P \leq 0.05$.

Isolate code	Absorbance (OD)	Concentration (µg/L)
RS3B	1.812 ± 0.02^{b}	2.93 ± 0.02^{ab}
RS3C	1.582 ± 0.04^{d}	2.55 ± 0.02^{d}
RS3D	1.295 ± 0.02^{e}	2.09 ± 0.05^{e}
RS3E	1.904 ± 0.03^{a}	3.07 ± 0.05^{a}
RS3F	1.944 ± 0.04^{a}	3.10 ± 0.05^{a}
RS4B	1.722 ± 0.05^{c}	2.78 ± 0.01^{bc}
RS4D	1.285 ± 0.05^{e}	2.08 ± 0.02^{e}
RS5D	1.847 ± 0.08^{ab}	2.98 ± 0.02^{ab}

Table 2. Quantitative analysis of phosphate solubilization. Mean values in each vertical column with the same lowercase letter(s) are not significantly different using Duncan's Multiple Range Test at $P \leq 0.05$.

Qualitative analysis of nitrogen fixing ability

Out of the 30 isolates evaluated for nitrogen fixing ability, it was only isolate RS3E that showed nitrogen-fixing potential by the appearance of a veil-like pellicle on LGI-P nitrogen-free semisolid medium as shown in Fig. 3.

Based on the results of these plant growth-promoting assays, isolate RS3F and RS3E were selected for further studies as the two of them had the highest PSI and also IAA producers, while isolate RS3E is the only nitrogen fixer and the highest phosphate solubilizer in liquid medium. The molecular identification of these two isolates were examined and were also used to synthesize selenium nanoparticles.

The produced IAA ranged from 0.339 ± 0.01^{d} to 1.182 ± 0.03^{a} (µg/mL). Isolates RS3F produced the highest concentration.

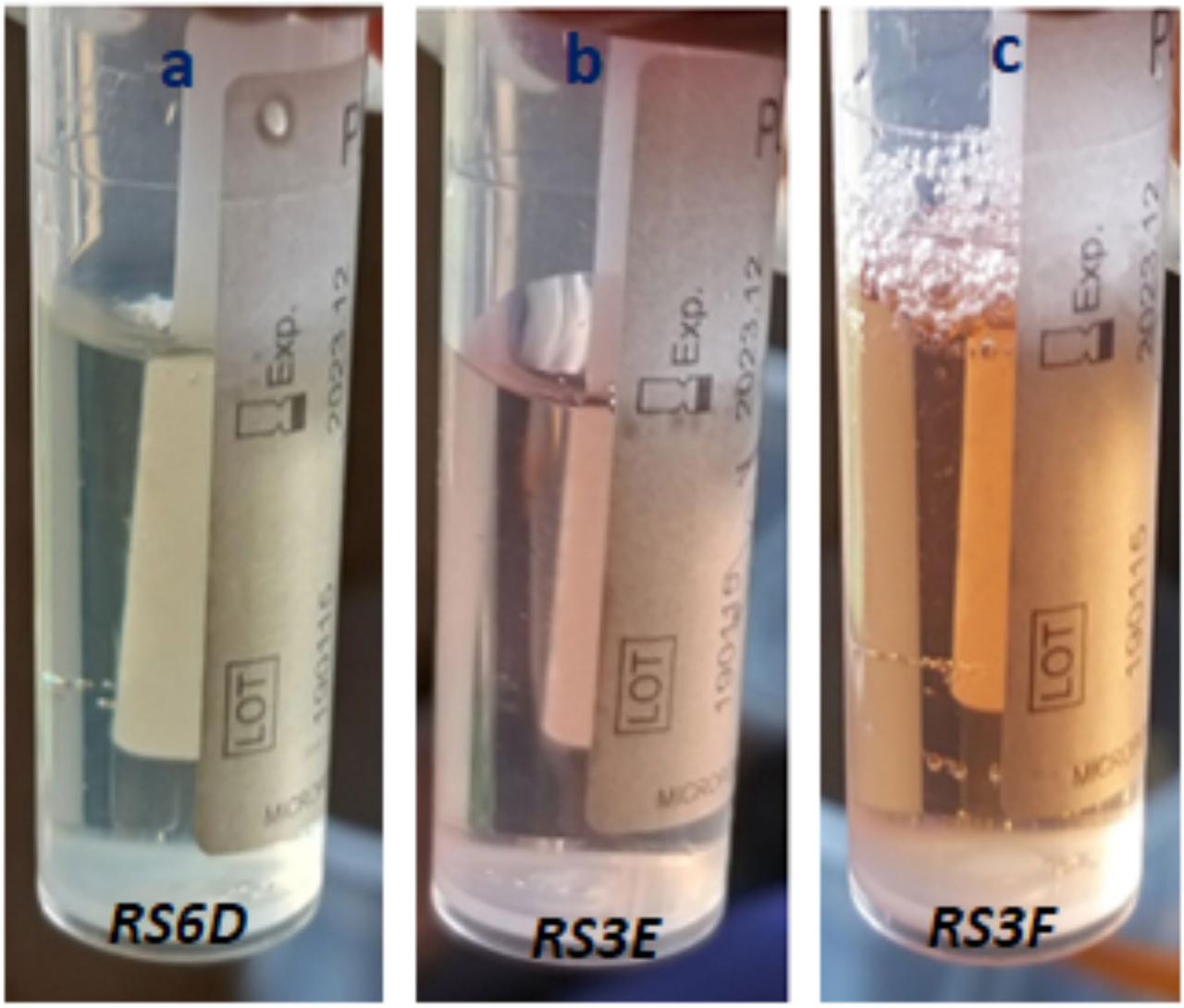

Fig. 2. (**a**–**c**) Indolic Compounds Production Assay: (**a**) Isolate RS6D (**b**) Isolate RS3E (**c**) Isolate RS3F. The intensity of pink coloration indicates the level of indolic compounds produced; a deeper pink signifies greater production.

Isolate code	Absorbance (at 530 nm)	Concentration (µg/mL)
RS1A	0.073 ± 0.01^{d}	0.428 ± 0.02^{cd}
RS1E	0.171 ± 0.02^{c}	0.625 ± 0.01^{bc}
RS3B	0.209 ± 0.02^{b}	0.702 ± 0.02^{b}
RS3F	0.446 ± 0.02^{a}	1.182 ± 0.03^{a}
RS4C	0.029 ± 0.01^{d}	0.339 ± 0.01^{d}
RS5B	0.275 ± 0.01^{b}	0.835 ± 0.04^{b}
RS5E	0.206 ± 0.01^{bc}	0.696 ± 0.01^{b}
RS6A	0.235 ± 0.01^{b}	0.754 ± 0.03^{b}
RS6D	0.058 ± 0.01^{d}	0.398 ± 0.01^{d}

Table 3. Indole acetic acid production concentration. Mean values in each vertical column with the same lowercase letter(s) are not significantly different using Duncan's Multiple Range Test at $P \leq 0.05$.

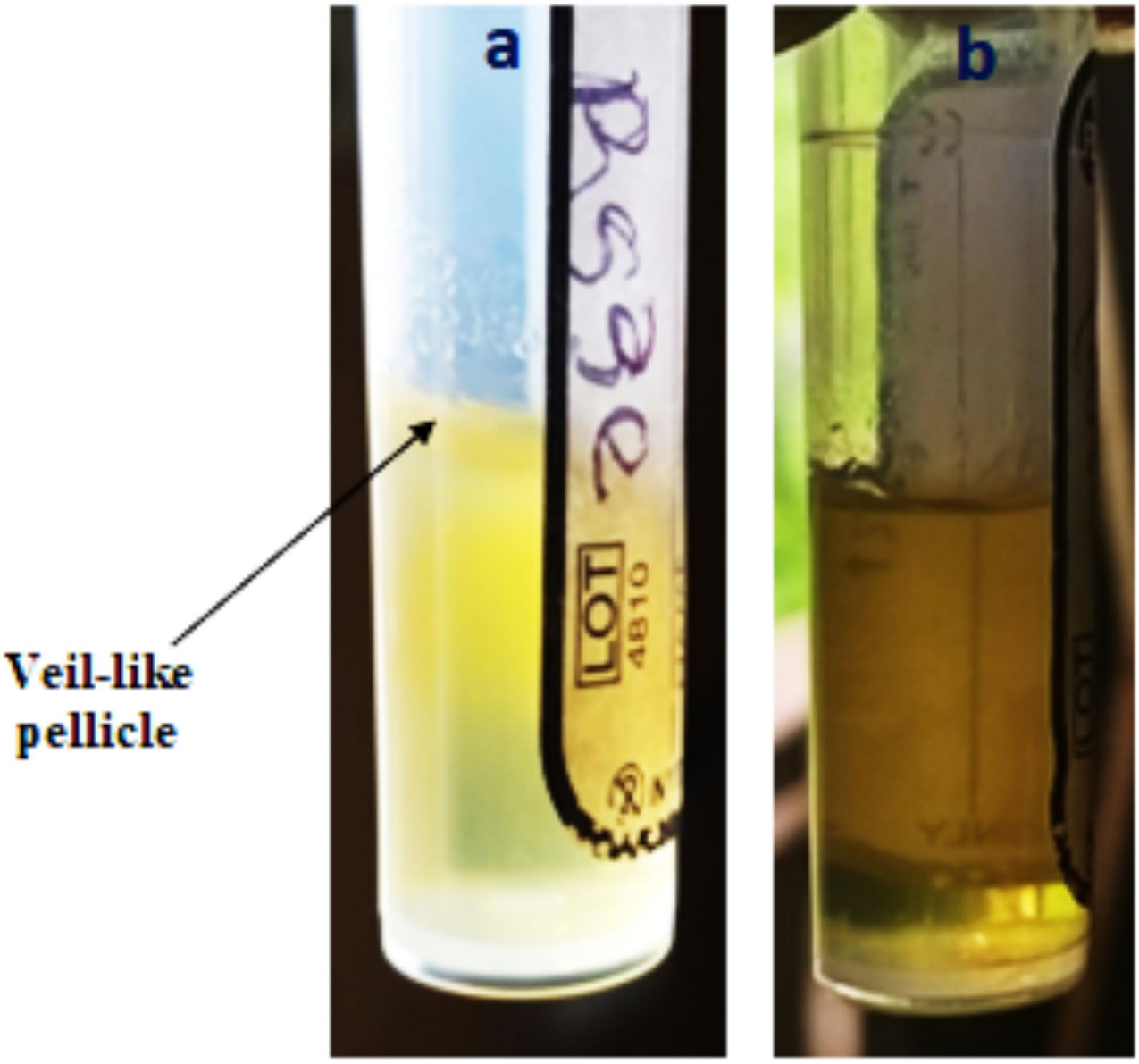

Fig. 3. (**a**–**b**) Development of Diazotrophs in LGI-P Nitrogen-Free Semi-Solid Media. (**a**) Isolate RS3E forms a veil-like pellicle near the media surface (indicated by the black arrow); (**b**) Control.

Molecular identification of the selected isolates

Figure 4: The neighbor-joining phylogenetic tree for the isolates RS3F and RS3E identified as *B. amyloliquefaciens* and *L. sphaericus*, respectively. This identification was based on the 16 S rRNA gene sequences and their corresponding accession numbers from NCBI. Percentages (≥ 90%) represent the frequency of taxa clustering in replicate trees from 1000 bootstrap tests. Evolutionary distances, calculated via the Tamura-Nei model, are expressed as base substitutions per site.

Synthesis and characterization of the biosynthesized senps

The UV-Vis absorption spectrum of the nanoparticles was examined between wavelengths 200–700 nm (Fig. 5a) after visual observation of the mixture at 72 h of incubation shown colour change from yellow to deep red (Fig. 5b). The greenly synthesized SeNPs had its maximum absorption at 262 nm.

The SEM analysis of the SeNPs revealed their spherical morphology, which was further corroborated by TEM images that also indicated some degree of agglomeration (Fig. 6a and b). The average estimated particle size (Do) was 16.704 nm, with a standard deviation (σ) of 1.328 nm (Fig. 6c). This was calculated by applying a log-normal function distribution to fit the particle distribution histogram.

The FTIR spectrum of the biosynthesized SeNPs, measured at wave numbers ranging from 4400 to 350 cm^{-1}, is shown in Fig. 7a. The FTIR spectra displayed nine peaks. Short vibrations between 4189.00 and 3883.70 cm^{-1}, along with sharp and broad vibrations between 3642.74 and 3446.33 cm^{-1}, indicate the presence of O–H

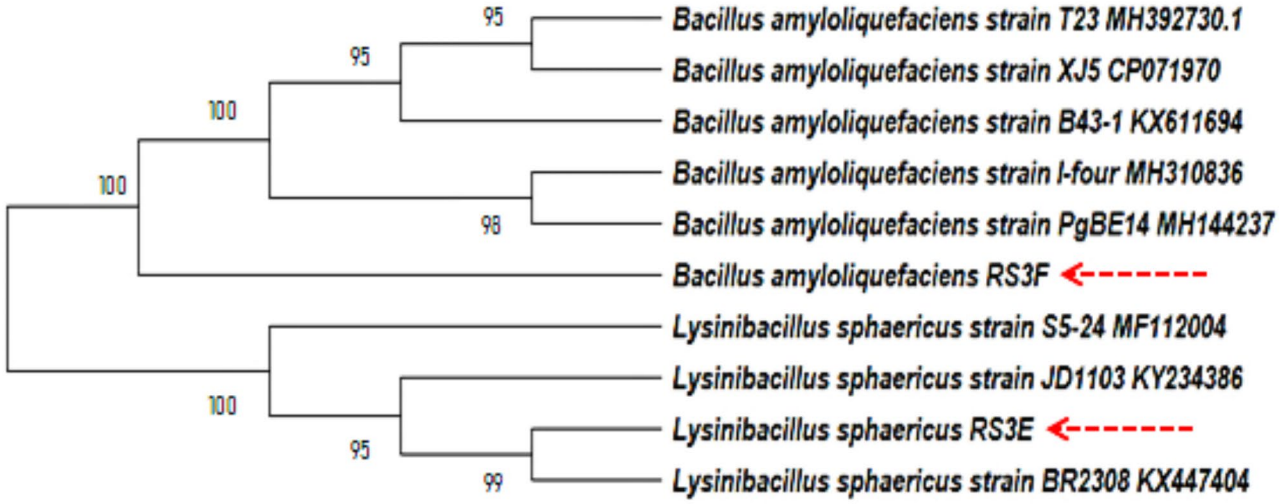

Fig. 4. illustrates the dendrogram representing the evolutionary relationships of the selected isolates RS3E and RS3F, along with closely related strains. This tree is based on 16 S rRNA gene sequences obtained from NCBI GenBank, which confirm the identification of the isolates as *Bacillus amyloliquefaciens* RS3F (accession number: PP747661) and *Lysinibacillus sphaericus* RS3E (accession number: PP747662).

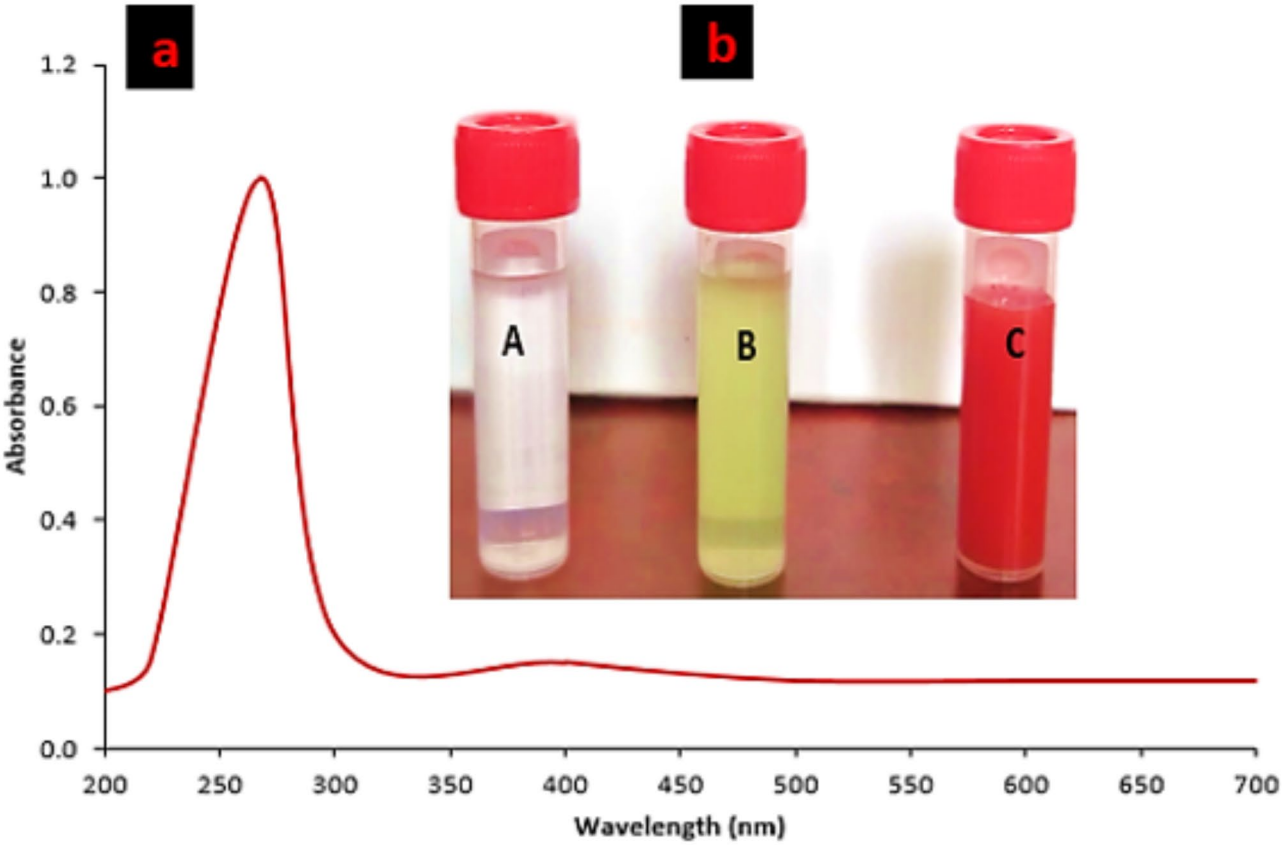

Fig. 5. (**a**) UV-Vis absorption spectrum of selenium nanoparticles synthesized using green methods. (**b**) Visual examination of the greenly synthesized selenium nanoparticles (SeNPs) after 72 h. at 36 °C. **A** = Sodium selenite dissolved in water; **B** = PGPR metabolite plus sodium selenite. **C** = Selenium nanoparticles (SeNPs) after incubation.

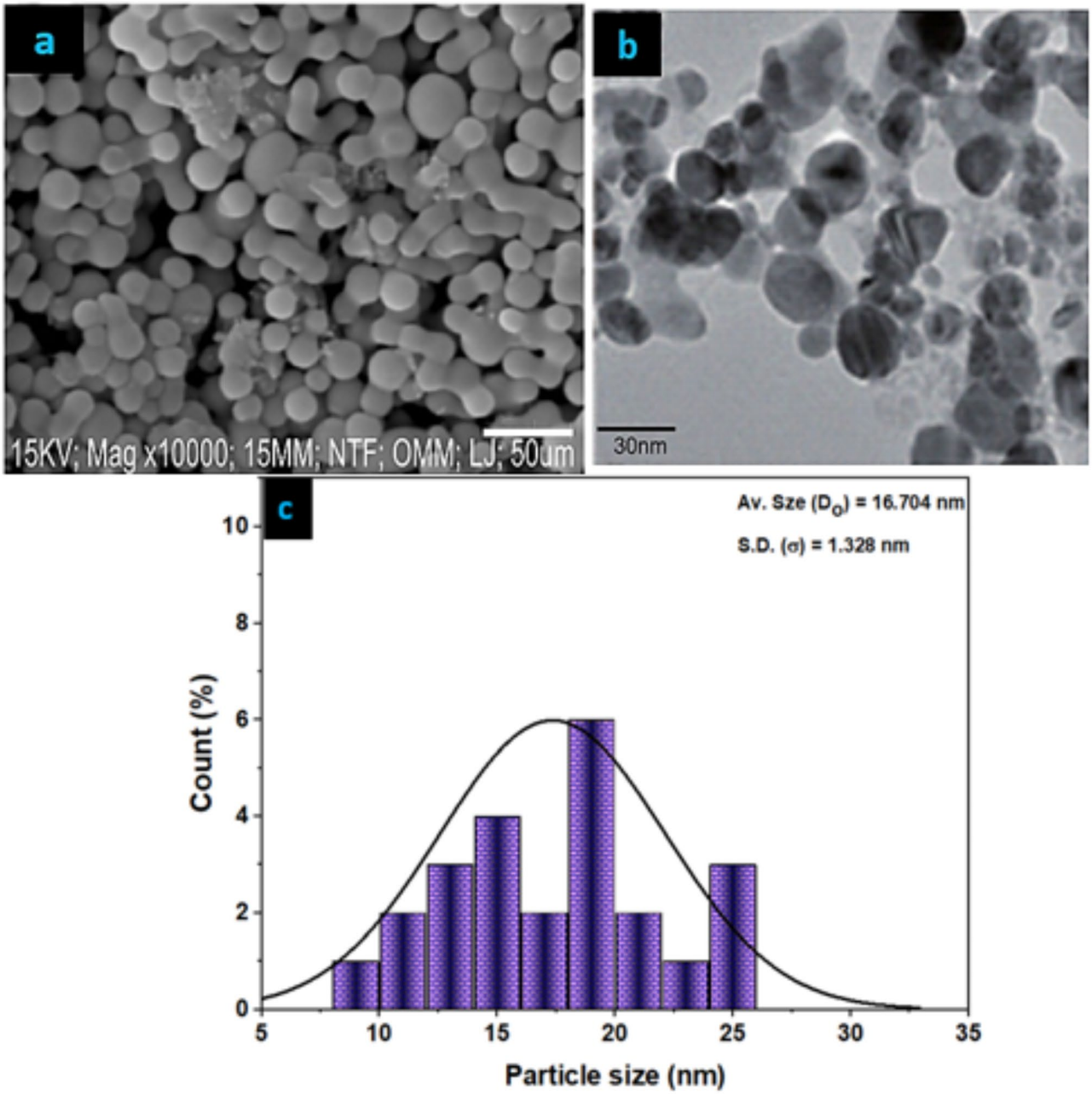

Fig. 6. (**a**) Scanning Electron Micrograph of the greenly synthesized SeNPs showing its spherical morphology; (**b**) Transmission Electron Micrograph of the greenly synthesized SeNPs; (**c**) Particle size distribution fitted with a log normal distribution function of the biosynthesized SeNPs.

stretching vibrations from free alcohol groups and intermolecularly-bonded alcohol groups. These groups can interact with the SeNPs through hydrogen bonding, contributing to their stabilization in solution. A medium peak between 2970.34 and 2871.58 cm^{-1} indicates the presence of C–H stretching vibrations from alkane groups, which provide hydrophobic interactions that help in creating a protective layer around the nanoparticles, thereby enhancing their dispersion in aqueous media. A moderate vibration at 1796.32 cm^{-1} indicates the presence of C=O stretching vibrations from carbonyl groups. These groups can coordinate with selenium atoms through electrostatic interactions, contributing to the stabilization of the SeNPs. The C–N stretch at 1642.74 cm^{-1} suggests the presence of amine groups (–NH2) or amide groups (–CONH–). These groups can form coordinate bonds with selenium atoms, further stabilizing the SeNPs. A robust and wide peak at 1435 cm^{-1} is associated with C–H bending or aromatic C=C stretching. A strong and distinct peak at 874.15 cm^{-1} indicates C–H out-of-plane bending vibrations, often found in aromatic compounds. The significant vibrations at 556.66 and 485.00 cm^{-1} are indicative of metal–oxygen (M–O) stretching vibrations, suggesting the interaction between selenium and stabilizing agents.

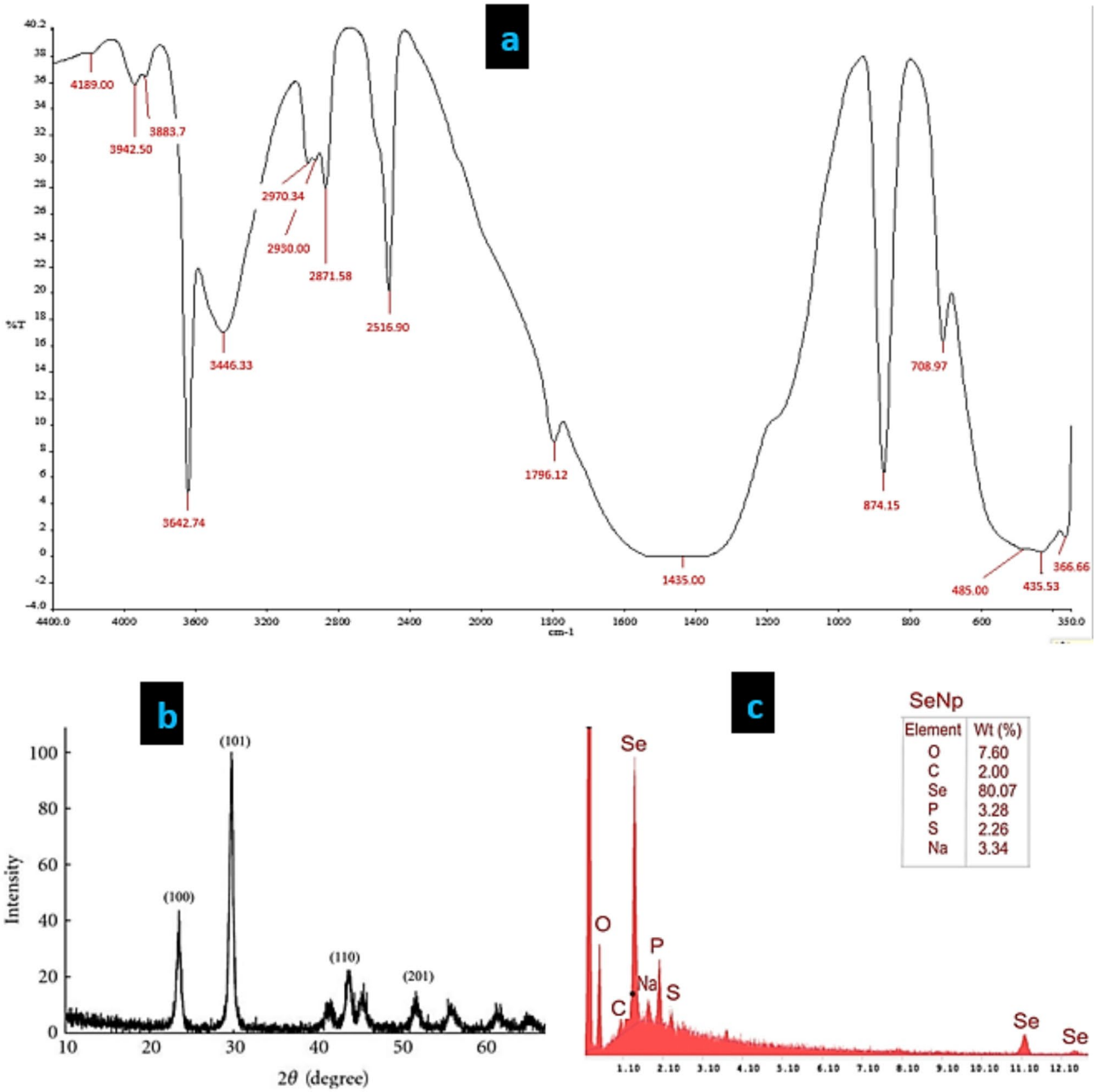

Fig. 7. (**a**) FTIR spectra of the greenly synthesized SeNPs; (**b**) XRD of the greenly synthesized SeNPs; (**c**) EDX showing the elemental composition of the greenly synthesized SeNPs.

The characteristics of the crystalline phase are illustrated in the XRD pattern, which corresponds to the face-centered cubic structure of the Bragg reflection index of BSNPs, as depicted in Fig. 7b. The XRD pattern reveals four significant peaks at 2θ values of 23.50°, 30.5°, 45.45°, and 52.5°. These peaks are identified as the (100), (101), (110), and (201) planes of the face-centered cubic (FCC) structure, respectively.

The qualitative and quantitative elemental composition of the biosynthesized NPs was analyzed using Energy dispersive x-ray diffraction (EDX), as shown in Fig. 7c. The elemental analysis confirmed the presence of SeNPs at a percentage of 80.07%. EDX spectra also showed the presence of SeNPs, which peaked at nearly 1.5 keV, indicating that selenium is the major element. The EDX analysis also showed that oxygen, carbon, phosphorus, sulphur, and sodium were present in the sample with varying concentrations, which is indicative of the capping and stabilizing agents present on the nanoparticles. The absence of additional elemental peaks and the significant presence of selenium in the spectra indicate the purity of the selenium metal in the transformed product.

Antifungal activity of the synthesized senps

The antifungal activity of the greenly synthesized SeNPs against the three selected phytopathogens is shown in Fig. 8. The synthesized NPs by RS3E, RS3F, and sodium selenite (control) were effective against *A. niger and A.*

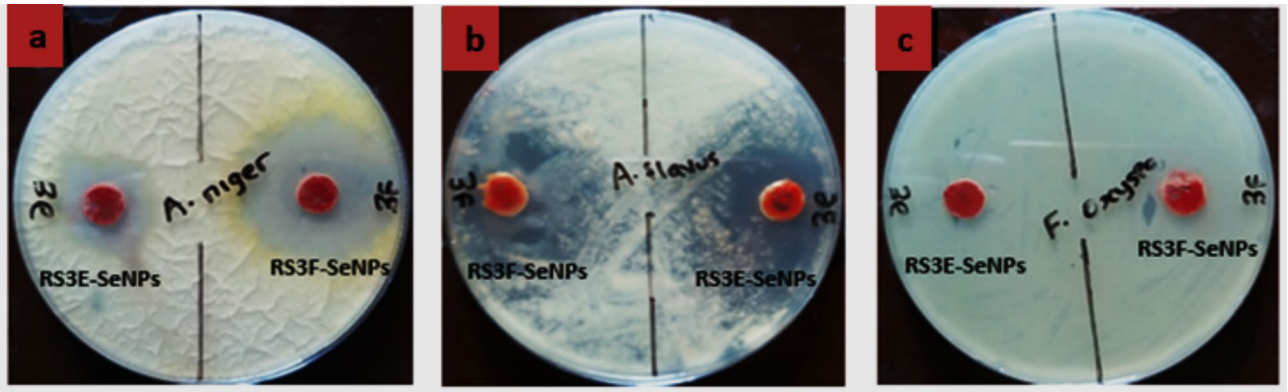

Fig. 8. Antifungal activity of the greenly synthesized SeNPs. Code: (**A**) = *Aspergillus niger;* (**B**) = *Aspergillus flavus;* (**C**) = *Fusarium oxysporum*.

	Antifungal activity (mm)		
Phytopathogens	**NaSe**	**RS3F-SeNPs**	**RS3E-SeNPs**
Aspergillus niger	10.0 ± 0.05^{c}	35.0 ± 0.08^{a}	23.0 ± 0.13^{b}
Aspergillus flavus	12.0 ± 0.11^{c}	40.0 ± 0.31^{b}	45.0 ± 0.18^{a}
Fusarium oxysporum	0.0 ± 0.00	0.0 ± 0.00	0.0 ± 0.00

Table 4. Antifungal activity of selenium nanoparticle (SeNPs) synthesized from selected PGPR metabolites. Mean values in each horizontal column with the same lowercase letter(s) are not significantly different using Duncan's Multiple Range Test at $P \leq 0.05$. Code: NaSe - Sodium Selenite; RS3F-SeNPs - Selenium nanoparticle synthesized by isolate RS3F; RS3E-SeNPs - Selenium nanoparticle synthesized by isolate RS3E, No Activity.

flavus and ineffective against *F. oxysporum*. The zones of inhibition ranged from 0.0 ± 0.00 to 45.0 ± 0.18^{a} mm as shown in Table 4. Against *A. niger*, RS3F-SeNP showed the highest (35.0 ± 0.08^{a} mm) while NaSe was the lowest (10.0 ± 0.05^{c}), and against *A. flavus*, RS3E-SeNP (45.0 ± 0.18^{a} mm) showed the highest antagonism while NaSe was the lowest (12.0 ± 0.11^{c}). The selenium nanoparticle showed no activity against *F. oxysporum*.

Discussions

Rhizobacteria promoting plant growths were isolated from the monkey pod tree rhizosphere. Their phosphate solubilization ability was evidenced by halo zone formation on PVK agar medium. Investigations on agar plates indicated that the clear zones created by phosphate-solubilizing microorganisms result from the production of organic acids or the release of alkaline phosphatase enzymes into the surrounding medium. This process lowers the pH of the medium, facilitating the chelation and solubilization of insoluble tricalcium phosphate[26,38,39].

In contrast to this study, Sanjotha and Manawadi[40] also screened for phosphate solubilizing bacteria; however, they used PVK (Pikovskaya's) and NBRIP (National Botanical Research Institute's phosphate growth) media, and reported more phosphate solubilizing isolates on NBRIP medium indicating that NBRIP medium was more efficient in screening for phosphate solubilizing organism compared to PVK medium. Nautiyal[26] conducted a study demonstrating that the yeast extract present in the PVK medium inhibited phosphate solubilization. As a result, yeast extract was removed from the PVK medium to create a new formulation without it. Subsequently, Mehta and Nautiyal[41] developed a defined microbiological growth medium called NBRIP, which does not contain yeast extract and is more effective than PVK for screening phosphate-solubilizing microorganisms. This new medium also requires the addition of a pH indicator dye, such as bromophenol blue or bromocresol purple, which changes colour as the pH decreases, allowing for easy visual assessment of phosphate-solubilizing efficiency.

The highest phosphate solubilizing index (PSI) was recorded for isolates RS3F, RS3C, and RS3D, with values of 3.80, 3.0, and 2.8, respectively. Solubilization efficiency was assessed using Nautiyal[26] scale, which classifies solubilizers into four categories: very low (< 1.0), low (1.0–2.0), medium (2.0–3.0), and high (> 3.0).The variation in phosphate solubilization potential, as indicated by the calculated PSI on agar plates, may be attributed to the relative strength, quantity, and diffusion rates of different organic acids, or to the effectiveness of alkaline phosphatase enzymes secreted by the bacterial isolates [42,43,44].

The observed broad range of phosphate solubilizing index (PSI), from 2.0 mm to 3.83 mm in this study, indicates diversity in the potential of the isolates to mobilize phosphate from insoluble sources. This variability is not uncommon and may reflect differences in microbial strains, growth conditions, and the mechanisms they employ to solubilize phosphate. Phosphate solubilizing microorganisms (PSMs) are known to secrete organic acids such as citric acid, gluconic acid, and acetic acid, which play a crucial role in dissolving insoluble phosphates and making them available to plants [45,46]. However, the efficiency of these microbes can differ

significantly depending on factors like the type of phosphate source, pH, temperature, and the presence of other microorganisms [45]. Bakki et al.[47] reported that *Bacillus* and *Pseudomonas* strains, which are well-known phosphate solubilizers, exhibited solubilization zones ranging from 1.08 to 6.69 mm on agar plates with tricalcium phosphate as the sole phosphorus source. This aligns with the solubilization range observed in our study (2.0–3.83 mm) and suggests that the isolates from the Monkey Pod tree may exhibit comparable solubilization capacities to these efficient phosphate solubilizers. Similarly, Aliyat et al. [48] reviewed the performance of phosphate solubilizing bacteria (PSB) and their role in soil fertility, indicating that phosphate solubilization potential typically ranges from 2.77 to 4.79 mm, similar to the results we have obtained. The authors pointed out that microbial diversity in the rhizosphere could contribute to such variability, making it essential to assess multiple isolates for agricultural efficacy.

Variable concentrations of soluble phosphorus (P) were released from $Ca_3(PO_4)_2$ by the bacterial isolates; however, there is a trend reversal when quantifying for the amount of soluble P released in the medium. Unlike isolates RS3F, RS3C, and RS3D having the highest PSI on agar plates, isolates RS4D, RS3E, and RS5D had the highest amount of solubilized P in liquid medium at 3.1, 3.07, and 2.98 respectively even though they had lower PSI on agar plates. Bechtaoui et al.[29] reached comparable conclusions and proposed that organic acids are not the sole means by which microorganisms solubilize phosphates. They indicated that the protons linked to extracellular polysaccharides released by these microorganisms also contribute to the dissolution of phosphate in liquid media.

In the assessment of indole acetic acid production, it was noted that phosphate solubilization and indole acetic acid production were almost mutually exclusive traits among the isolates. Only one phosphate solubilizer, RS3F, was found to produce indole acetic acid at the highest concentration of 1.182 µg/mL, followed by isolate RS5B, which had a concentration of 0.835 µg/mL however with lower PSI than isolate RS3E. These findings align with those reported by Myo et al.[49], which showed concentrations of 0.791 µg/mL and 1.052 µg/mL, but are lower than the values reported by Nakurte et al.[50], which were 1.152 µg/mL and 1.425 µg/mL.

In this study, the IAA production by the isolates ranged from 0.339 ± 0.01 to 1.182 ± 0.03 µg/mL, with isolate RS3F exhibiting the highest concentration. These findings indicate that both isolates exhibit moderate to strong IAA-producing potential, a key trait of PGPB. The ability of these isolates to synthesize IAA can positively impact plant growth by promoting root development, improving nutrient uptake, and enhancing overall plant health. Sethia et al. [51] reported that *Pseudomonas fluorescens* strains produce IAA concentrations ranging from 0.5 µg/mL to 2.0 µg/mL, supporting the observation that the IAA levels of isolates RS3E and RS3F fall within the expected range for effective PGPB. In contrast, Jensen et al.[52] reported a higher IAA concentration of 3.63 µg/mL in *Bacillus subtilis* ALC_02 strains.

The variations in production can be linked to different environmental sources and the significant diversity among bacterial isolates[53]. The synthesis of indole acetic acid is indicative of plant growth-promoting properties, implying that organisms capable of producing this compound can enhance plant development [49,54]. Tryptophan is naturally released in the root exudates of plants, and it is widely believed that most of the auxin present in the rhizosphere originates from biosynthesis by microorganisms[24,55].

The nitrogen-fixing potential of the rhizobacterial isolates was evaluated using LGI-P semi-solid medium at pH 5.5, devoid of nitrogen. In this medium, motile aerotactic diazotrophs form a pellicle under microaerobic conditions (low oxygen levels), which are conducive to nitrogen fixation[56]. The primary enzymatic complex responsible for biological nitrogen fixation is nitrogenase, whose synthesis and activity are tightly regulated by the presence of ammonium and oxygen[25]. Only isolate RS3E was able to fix nitrogen in this study. This is in contrast to the work of Gupta and Gupta, [35], where they reported nine nitrogen-fixing rhizobacterial isolates. The disparity in results could be due to the difference in isolation site and the methodology used to assay for the activity[57].

The two most effective PGPR isolates, RS3E and RS3F, were selected and successfully utilized for the biosynthesis of selenium nanoparticles. The synthesis was initially indicated by a red colour shift in the reaction mixture, which was later confirmed through characterization of the green-synthesized nanoparticles. As described by Puri and Patil[58], the transition from dark brown to ruby red in the reaction mixture signifies the successful synthesis of selenium nanoparticles. This change is a common indicator used in nanoparticle synthesis protocols, particularly those involving natural extracts [59]. The UV-Vis absorption spectrum of the selenium nanoparticle showed peak absorption at 268 nm and the spherical nature of the nanoparticle was confirmed using SEM. Similar to this finding, Ramachandran et al.[60] reported 264 nm as the peak for the SeNPs by *Bacillus* sp. MKUST-01 exopolysaccharide. This specific absorption wavelength aligns with the characterization of selenium nanoparticles. Such UV-Vis spectra are essential for confirming the unique optical properties of these nanostructures, indicative of their size and composition[60].

Selenium nanoparticles (SeNPs) have attracted considerable interest because of their promising applications across multiple domains, such as agriculture, pharmaceuticals, medicine, and environmental cleanup. The biosynthesis of SeNPs using bacteria, particularly *Bacillus* sp., has been extensively studied due to its eco-friendly and cost-effective nature. The characterization of SeNPs synthesized by *Bacillus* sp. is crucial to understand their properties and potential applications [61].

TEM and SEM are commonly used techniques to analyze the morphology and size distribution of SeNPs. They reveal the shape, size, morphology at a nanoscale level, and topographical information illustrating the external structure and surface properties. The spherical morphology observed in this study is similar to what was reported by Ullah et al.[62] and Adeniran et al. [37]. However, Kora and Rastogi[63] and Ullah et al.[62] respectively reported lower and higher SEM and TEM sizes for the selenium nanoparticles synthesized by *Escherichia coli* ATCC 35,218 and *Bacillus subtilis* BSN313 and found that the average particles were 155 and 530 nm. In another study, Wang et al. [64] reported 239.6 nm particle size for the SeNPs synthesised by *Pediococcus acidilactici* DSM20284.

FTIR spectroscopy is a valuable technique used to analyze the functional groups and chemical bonds on the surface of SeNPs by the rhizobacteria, confirming the presence of biomolecules involved in nanoparticle synthesis. Overall, the SeNPs was shown to contain capping layers of proteins, polysaccharides and lipids. Kamnev et al.[65] and Tugarova et al. [66] used FTIR spectroscopy to analyze SeNPs synthesized by *Bacillus subtilis* SE201412 and *Azospirillum thiophilum* and found that the particles were surrounded by proteins and polysaccharides, which played a role in the stability and reduction of selenite to SeNPs.

EDX was employed to analyze the elemental composition of SeNPs, confirming their purity and chemical composition. The results indicated that the nanoparticle sample contained 80.07% selenium and 19.03% of other elements. These additional elements included oxygen, carbon, phosphorus, sulfur, and sodium, which suggest the presence of capping agents on the selenium nanoparticles. Similarly, studies by Kora and Rastogi[63] and Ullah et al.[62] utilized EDX to characterize selenium nanoparticles synthesized by *Escherichia coli* ATCC 35,218, confirming that the particles were predominantly composed of pure selenium.

XRD analysis is employed to determine the crystalline structure, size, and phase of SeNPs, which are critical for understanding their physical properties. In a study similar to this one, Che et al.[67] used XRD to analyze SeNPs synthesized by *Lysinibacillus sp.* ZYM-1 and reported that the particles exhibited a spherical crystalline structure. In contrast, Liu et al.[68] observed a hexagonal crystalline structure in SeNPs synthesized by *Bacillus paramycoides* using XRD analysis.

The antifungal activity of SeNPs biosynthesized by PGPR isolates RS3E and RS3F, evaluated against phytopathogens, demonstrated that the green-synthesized nanoparticles were effective against *A. niger* and *A. flavus*, producing inhibition zones ranging from 35.0 ± 0.05 mm to 45.0 ± 0.18 mm. Similar findings have been reported for SeNPs synthesized by *Bacillus sp.* MSh-1 and *Delftia sp.* 5, which exhibited inhibitory effects against *A. fumigatus*, *Candida albicans*, and the wood-rotting fungus *Ophiostoma pelliculosum* [23,69]. Additionally, SeNPs synthesized using the leaves of *Melia azedarach* were effective against *Fusarium mangiferae*, a causative agent of mango malformation disease[70]. However, in the present study, the SeNPs were ineffective against *F. oxysporum*. This observation aligns with previous findings that demonstrated selective antifungal activity of SeNPs depending on the fungal species. For example, SeNPs synthesized by the cyanobacterium *Desmonostoc alborizicum* were effective against *Alternaria alternata*, while *Pythium ultimum* exhibited significant resistance[22]. In contrast, other studies have shown efficacy of SeNPs synthesized from *Amphipterygium glaucum* leaves and *Calendula officinalis* flowers against *F. oxysporum* at higher concentrations (0.25 mg/mL)[21].

The differential susceptibility of the fungi in this study can be attributed to multiple factors, including the physicochemical properties of the SeNPs, such as size, surface charge, and functional group coatings, as well as fungal-specific resistance mechanisms[21,71]. The SeNPs in this study had an average size of 16.704 nm, a range considered effective for interacting with fungal cell membranes. Smaller nanoparticles possess a higher surface-to-volume ratio, enhancing their ability to generate reactive oxygen species (ROS) and interact with fungal cell walls[72]. However, *F. oxysporum* has a robust cell wall composition enriched with chitin and β-glucans, which might hinder the penetration of even small nanoparticles[73]. The FTIR analysis indicated the presence of organic molecules coating the nanoparticles, which could enhance interactions with fungal membranes. Positively charged SeNPs typically exhibit stronger electrostatic interactions with negatively charged fungal cell walls[74]. Therefore, if the SeNPs in this study were neutral or negatively charged, their effectiveness against *F. oxysporum* may have been reduced. SeNPs are also known to induce oxidative stress in fungal cells by generating ROS, which disrupt cellular components, including membranes, proteins, and DNA [75]. The susceptibility of *A. niger* and *A. flavus* to this oxidative damage suggests a weaker antioxidant defense system compared to *F. oxysporum*, which likely possesses robust mechanisms (e.g., catalase and superoxide dismutase enzymes) to neutralize ROS[76]. This fungus may produce extracellular enzymes that degrade or inactivate nanoparticles. Additionally, the genetic adaptability of *F. oxysporum* may have enabled it to develop specific resistance pathways, such as efflux pumps or protective biofilm formation, which reduce the efficacy of SeNPs.

Conclusion

This study highlights the dual significance of rhizobacteria in promoting plant growth and serving as biological platforms for the synthesis of SeNPs with antifungal potential. The isolation of rhizobacterial strains RS3E and RS3F, identified as *Lysinibacillus sphaericus* and *Bacillus amyloliquefaciens*, underscores the rich microbial diversity in the rhizosphere of monkey pod trees. These strains exhibited significant phosphate solubilization and indole acetic acid production, key mechanisms for enhancing nutrient availability and hormone regulation in plants. These findings reaffirm the pivotal role of plant growth-promoting rhizobacteria in sustainable agriculture by reducing dependence on chemical fertilizers and supporting eco-friendly practices.

The successful green synthesis of SeNPs by these rhizobacterial strains represents a novel integration of microbiology and nanotechnology. The SeNPs were characterized as spherical with an average particle size of 16.704 nm, as confirmed by SEM, TEM, FTIR, XRD, and EDX analyses. These nanoparticles demonstrated significant antifungal activity against *Aspergillus niger* and *Aspergillus flavus*, revealing their potential as eco-friendly antifungal agents. However, their ineffectiveness against *Fusarium oxysporum* highlights the need for further exploration of nanoparticle properties and fungal resistance mechanisms.

The development of antimicrobial and antifungal agents faces several challenges, including the emergence of resistant pathogens, environmental toxicity, and the high cost of chemical synthesis. SeNPs address these challenges through their biocompatibility, low toxicity, and potential to disrupt fungal cell membranes and generate reactive oxygen species (ROS), mechanisms that minimize resistance development. Moreover, their green synthesis using rhizobacteria offers an eco-friendly and cost-effective alternative to conventional methods. This approach aligns with global efforts to combat agricultural pathogens while reducing environmental impact.

Future studies should focus on optimizing SeNPs synthesis to enhance antifungal efficacy, particularly against resistant fungi such as *Fusarium oxysporum*. Additionally, incorporating reference standards like

amphotericin B or fluconazole will be crucial for validating and quantifying the relative effectiveness of SeNPs. Furthermore, investigating the synergistic effects of SeNPs with conventional fungicides and exploring their broader applications in agriculture and medicine could provide innovative solutions to current antimicrobial challenges.

Data availability

The sequences of Bacillus amyloliquefaciens RS3F and Lysinibacillus sphaericus RS3E were deposited in the NCBI GenBank database (https://www.ncbi.nlm.nih.gov/) under accession number PP747661 and PP747662 respectively. All raw data are available upon request from the corresponding author.

Received: 5 September 2024; Accepted: 27 March 2025
Published online: 14 May 2025

References

1. Bhat, M. A. et al. *Plants* **12**(3), 629. https://doi.org/10.3390/plants12030629. (2023).
2. Rehan, M., Al-Turki, A., Abdelmageed, A. H. A., Abdelhameid, N. M. & Omar, A. F. *Plants* **12**(8), 1588. https://doi.org/10.3390/plants12081588. (2023).
3. Zaidi, A., Khan, M. S., Ahemad, M. & Oves, M. *Acta Microbiol. Immunol. Hung.* **56**(3), 263–284. https://doi.org/10.1556/AMicr.56.2009.3.6 (2009).
4. Sun, W., Shahrajabian, M. H. & Soleymani, A. *Plants* **13**(5), 613. https://doi.org/10.3390/plants13050613 (2024).
5. Saeed, Q. et al. *Int. J. Mol. Sci.* **22**(19), 10529. https://doi.org/10.3390/ijms221910529. (2021).
6. Olanrewaju, O. S., Glick, B. R. & Babalola, O. O. Mechanisms of action of plant growth promoting bacteria. *World J. Microbiol. Biotechnol.* **33**(11), 197. https://doi.org/10.1007/s11274-017-2364-9 (2017).
7. Timofeeva, A. M., Galyamova, M. R. & Sedykh, S. E. *Plants* **12**, 4074. (2023). https://doi.org/10.3390/plants12244074
8. Fahde, S., Boughribil, S., Sijilmassi, B. & Amri, A. *Agricul* **13**, 1279. https://doi.org/10.3390/agriculture13071279. (2023).
9. Delgado, D. C., Hera, R., Cairo, J. & Orta, Y. *Cuban J. Agricul Sci.* **48**(3), 205–212. https://cjascience.com/index.php/CJAS/article/view/573 (2014).
10. Sati, D., Pande, V., Pandey, S. C. & Samant, M. *J. Soil. Sci. Plant. Nutr.* **23**, 106–124. https://doi.org/10.1007/s42729-021-00724-5 (2023).
11. CTE (Cameroon Timber Export), (Accessed 25. Aug. (2022). www.cameroontimberexport.com/monkey-pod-wood/
12. Kang, Y. et al. *J. Agricul Food Chem.*, **72**(3), 1473–1486. https://doi.org/10.1021/acs.jafc.3c07504. (2024).
13. AbdElgawad, H. et al. *ACS Omega* **8**(29), 26414–26424. https://doi.org/10.1021/acsomega.3c02957 (2023).
14. Thabet, S. G. & Alqudah, A. M. *Plant Soil.* (2024). https://doi.org/10.1007/s11104-024-06581-2
15. Tendenedzai, J. T., Chirwa, E. M. N. & Brink, H. G. *Sci. Rep.* **13**(1), 20379. https://doi.org/10.1038/s41598-023-47616-5. (2023).
16. Corbu, V. M., Gheorghe-Barbu, I., Dumbravă, A. Ş., Vrâncianu, C. O. & Şesan, T. E. *Microorganisms* **11**(6), 1384. https://doi.org/10.3390/microorganisms11061384 (2023).
17. Ekwomadu, T. I. & Mwanza, M. *Agriculture* **13**(9), 1810. https://doi.org/10.3390/agriculture13091810 (2023).
18. Zakaria, L. *Pathogens* **13**(9), 813. https://doi.org/10.3390/pathogens13090813 (2024).
19. Islam, T., Tamanna, N. T., Matin, M. N., Barai, H. R. & Haque, M. A. *Plants* **13**(19), 2737. https://doi.org/10.3390/plants13192737 (2023).
20. Shahbaz, M. et al. *Plants* **12**(4), 761. https://doi.org/10.3390/plants12040761. (2023a).
21. Lazcano-Ramírez, H. G. et al. *Antibiotics* **12**(1), 115. https://doi.org/10.3390/antibiotics12010115. (2023).
22. Nowruzi, B., Jalil, B. S. & Metcalf, J. S. *BMC Biotechnol.* **23**(1), 41. https://doi.org/10.1186/s12896-023-00807-4. (2023).
23. Pescuma, M. et al. *Biotechnol. Rep.* **37**, e00787. https://doi.org/10.1016/j.btre.2023.e00787. (2023).
24. Kaur, T., Rani, R. & Manhas, R. K. *AMB Express* **9**(1), 125. https://doi.org/10.1186/s13568-019-0849-7 (2019).
25. Ambrosini, A. & Passaglia, L. M. P. *Curr. Protocols Plant. Biol.* **2**(3), 190–209. https://doi.org/10.1002/pb.20054 (2017).
26. Nautiyal, C. S. *FEMS Microbiol Lett* **170**, 265–270. (1999). https://doi.org/10.1111/j.1574-6968.1999.tb13383.x
27. Elias, F., Woyessa, D. & Muleta, D. *Int. J. Microbiol.* **2016**, 5472601. (2016). https://doi.org/10.1155/2016/5472601
28. S.R. Olsen, and Sommers, L.E. (1982). Part 2. Chemical and Microbiological Properties, Agronomy Monographs 9, 2nd Edition, ASA and SSSA, Madison, 403–430. https://doi.org/10.2134/agronmonogr9.2.2ed.c24.
29. Bechtaoui, N. et al. M., and *Biol. Open.* **8**(7), bio043968. https://doi.org/10.1242/bio.043968 (2019).
30. Argolo, C. S., Argôlo-Filho, R. C. & Loguercio, L. L. *BMC Microbiol. 19*. (2019). https://doi.org/10.1186/s12866-019-1446-2
31. Fardsadegh, B. & Jafarizadeh-Malmiri, H. *Green. Process. Syn.* **8**(1), 399–407. https://doi.org/10.1515/gps-2019-0007 (2019).
32. Ikram, M. et al. *Green. Process. Syn.* **9**(1), 706–714. https://doi.org/10.1515/gps-2020-0067. (2020).
33. Schiavon, M., Lima, L. W., Jiang, Y. & Hawkesford, M. J. *Plant Ecophysiol.* 11 (Springer, 2017). https://doi.org/10.1007/978-3-319-56249-0_15
34. Mroczek-Zdyrska, M. & Wójcik, M. *Biol. Trace Elem. Res.* **147**(1–3), 320–328. https://doi.org/10.1007/s12011-011-9292-6 (2012).
35. Gupta, M. & Gupta, S. *Front. Plant Sci.* **7** (2016). https://doi.org/10.3389/fpls.2016.02074
36. Diao, M. et al. *Plant. Growth Reg.* **33**(3), 671–682. https://doi.org/10.1007/s00344-014-9416-2 (2014).
37. Adeniran, O. A., Sanusi, J. F., Adebami, G. E. & Adebayo-Tayo, B. C. *J. Digit. Innov. Contemp. Res. Sci. Eng. Technol.* **10**(3), 17–32. https://doi.org/10.22624/AIMS/DIGITAL/V10N3P2. (2022).
38. Behera, B. C. et al. *J. Genet. Eng. Biotechnol.* **15**(1), 169–178. https://doi.org/10.1016/j.jgeb.2017.01.003. (2017).
39. Gupta, R. et al. *Saudi J. Biol. Sci.* **29**(1), 35–42. https://doi.org/10.1016/j.sjbs.2021.09.075. (2022).
40. Sanjotha, G. & Manawadi, S. *Int. J. Res. Stud. Microbiol. Biotechnol.* **2**(2), 1–6. https://doi.org/10.20431/2454-9428.0202001 (2016).
41. Mehta, S. & Nautiyal, C. S. *Curr. Microbiol.* **43**, 51–56. https://doi.org/10.1007/s002840010259 (2001).
42. Pande, A., Pandey, P., Mehra, S., Singh, M. & Kaushik, S. *J. Genet. Eng. Biotechnol.* **15**(2), 379–391. https://doi.org/10.1016/j.jgeb.2017.06.005 (2017).
43. Janati, W., Mikou, K., El Ghadraoui, L. & Errachidi, F. *Front. Microbiol.* **13**, 958300. https://doi.org/10.3389/fmicb.2022.958300. (2022).
44. EAP et al. *Front. Plant. Sci.* **14**, 1324056. https://doi.org/10.3389/fpls.2023.1324056. (2024).
45. Tian, J., Ge, F., Zhang, D., Deng, S. & Liu, X. *Biol* **10**(2), 158. https://doi.org/10.3390/biology10020158. (2021).
46. Iftikhar, A. et al. *Discov Appl. Sci.* **6**, 33 https://doi.org/10.1007/s42452-024-05683-x. (2024).
47. Bakki, M. et al. *Front. Microbiol.* **15**, 1289466. https://doi.org/10.3389/fmicb.2024.1289466 (2024).
48. Aliyat, F. Z., Maldani, M., Guilli, E., Nassiri, M. & Ibijbijen, J. L., and *Microorganisms* **10**(5), 980. https://doi.org/10.3390/microorganisms10050980 (2022).
49. Myo, E. M. et al. *BMC Microbiol.* **19**(1), 155. https://doi.org/10.1186/s12866-019-1528-1 (2019).
50. Nakurte, I., Keisa, A. & Rostoks, N. *J Anal Method Chem* **103575**, 1–6. (2012). https://doi.org/10.1155/2012/103575
51. Sethia Msethustafa, B., Manohar, M., Patil, S., Jayamohan, S. V. & Kumudini, N. S. B.S *Indian J. Exp. Biol.* **53**(6), 342–349. (2015)
52. Jensen, G. C. N. et al. *Physiol. Plant.* **176**(3), e14338. https://doi.org/10.1111/ppl.14338 (2024).

53. Khianngam, S., Meetum, P., Chiangmai, P. N. & Tanasupawat, S. *Trop. Lif Sci. Res.* **34**(1), 219–239. https://doi.org/10.21315/tlsr2023.34.1.12. (2023).
54. Etesami, H. & Glick, B. R. *Microbiol. Res.* **281**, 127602. https://doi.org/10.1016/j.micres.2024.127602. (2024).
55. Zhang, B. X. et al. *RSC Adv.* **11**(50), 31601–31607. https://doi.org/10.1039/d1ra05659j. (2021).
56. Tang, A., Haruna, A. O., Majid, N. M. A. & Jalloh, M. B. *Microorganisms* **8**(3), 442. https://doi.org/10.3390/microorganisms8030442. (2020).
57. Zhang, X., Tong, J., Dong, M., Akhtar, K. & He, B. *PeerJ* **10**, e12677. https://doi.org/10.7717/peerj.12677. (2022).
58. Puri, A. & Patil, S. *Biosci. Biotech. Res. Asia* **19**(2). https://doi.org/10.13005/bbra/2997. (2022).
59. Sampath, S., Sunderam, V., Manjusha, M., Dlamini, Z. & Lawrance, A. V. *Molecules* **29**, 801. https://doi.org/10.3390/molecules29040801. (2024).
60. Ramachandran, T. et al. *Biomedicines* **11**(9), 2520. https://doi.org/10.3390/biomedicines11092520. (2023).
61. Khaledizade, E., Tafvizi, F. & Jafari, P. *J. Trace Ele Med. Biol.* **82**, 127357. https://doi.org/10.1016/j.jtemb.2023.127357. (2024).
62. Ullah, A. et al. *Molecules* **26**(18), 5559. https://doi.org/10.3390/molecules26185559. (2020).
63. Kora, A. J. & Rastogi, L. *IET Nanobiotechnol.* **11**(2), 179–184. https://doi.org/10.1049/iet-nbt.2016.0011. (2017).
64. Wang, Q., Wang, C., Kuang, S., Wang, D. & Shi, Y. *Molecules* **28**(9), 3793. https://doi.org/10.3390/molecules28093793 (2023).
65. Kamnev, A. A. et al. *Molecules* **26**(4), 1146. https://doi.org/10.3390/molecules26041146 (2021).
66. Tugarova, A. V., Mamchenkova, P. V., Dyatlova, Y. A. & Kamnev, A. A.). *Part A. Molecul Biomolecul Spectr.* **192**, 458–463. https://doi.org/10.1016/j.saa.2017.11.050 (2018).
67. Che, L. et al. *ACS Sust Chem. Eng.* **5**(5), 2535–2543. https://doi.org/10.1021/acssuschemeng.6b02889 (2017).
68. Liu, P. et al. *Front. Bioeng. Biotechnol.* **11**, 1227619. https://doi.org/10.3389/fbioe.2023.1227619 (2023).
69. Shakibaie, M., Salari Mohazab, N., Ayatollahi Mousavi, S. A. & Jundishapur *J. Microbiol.* **8**(9), e26381. https://doi.org/10.5812/jjm.26381. (2015).
70. Shahbaz, M. et al. *PLOS ONE* **18**(2). https://doi.org/10.1371/journal.pone.0274679. (2023).
71. Mikhailova, E. O. *Molecules 28*(24). (2023). https://doi.org/10.3390/molecules28248125
72. Fallah, S., Yusefi-Tanha, E. & Peralta-Videa, J. R. *Plant. Nano Biology* **10**, 100105. https://doi.org/10.1016/j.plana.2024.100105 (2024).
73. Schoffelmeer, E. A. M., Sietsma, K. F. M. & Cornelissen, B. J. C. J. H. and *Fungal Genet. Biol.* **27**, 275–282 (1999). 1087–1845/99 $30.00.
74. Chen, Y., Liu, W., Leng, X. & Stoll, S. *Sci. Total Envion* **808**, 152010. https://doi.org/10.1016/j.scitotenv.2021.152010 (2022).
75. Ravi, D., Gunasekar, B., Kaliyaperumal, V. & Babu, S. *OpenNano* **20**, 100219. https://doi.org/10.1016/j.onano.2024.100219 (2024).
76. Mikhailova, E. O. *Molecules* **28**(24), 8125. https://doi.org/10.3390/molecules28248125 (2023).

Author contributions

B.C.A. conceived, designed, analyzed, and interpreted the data, and wrote the first draft of the paper; G.E.A. co-design, co-analyzed and interpreted the data, wrote the first draft of the paper, edited the drafted paper; A.M.B. performed the experiments, co-analyzed and interpreted the data. All the authors read and approved the final draft.

Funding

The authors did not receive support from any organization for the submitted work.

Declarations

Competing interests

The authors declare no competing interests.

Additional information

Correspondence and requests for materials should be addressed to G.E.A. or B.C.A.-T.

Reprints and permissions information is available at www.nature.com/reprints.

Publisher's note Springer Nature remains neutral with regard to jurisdictional claims in published maps and institutional affiliations.